ACS central science

Research Article

Cite This: ACS Cent. Sci. 2019, 5, 65−72

http://pubs.acs.org/journal/acscii

Effective Distance for DNA-Mediated Charge Transport between Repair Proteins

Edmund C. M. Tse,[†] Theodore J. Zwang,[‡] Sebastian Bedoya, and Jacqueline K. Barton*

Division of Chemistry and Chemical Engineering, California Institute of Technology, Pasadena, California 91125, United States

Supporting Information

ABSTRACT: The stacked aromatic base pairs within the DNA double helix facilitate charge transport down its length in the absence of lesions, mismatches, and other stacking perturbations. DNA repair proteins containing [4Fe4S] clusters can take advantage of DNA charge transport (CT) chemistry to scan the genome for mistakes more efficiently. Here we examine the effective length over which charge can be transported along DNA between these repair proteins. We define the effective CT distance as the length of DNA within which two proteins are able to influence their ensemble affinity to the DNA duplex via CT. Endonuclease III, a DNA repair glycosylase containing a [4Fe4S] cluster, was incubated with DNA duplexes of different lengths (1.5−9 kb), and atomic force microscopy was used to quantify the binding of proteins to these duplexes to determine how the relative protein affinity changes with increasing DNA length. A sharp change in binding slope is observed at 3509 base pairs, or about 1.2 μm, that supports the existence of two regimes for protein binding, one within the range for DNA CT, one outside of the range for CT; DNA CT between the redox proteins bound to DNA effectively decreases the ensemble binding affinity of oxidized and reduced proteins to DNA. Utilizing an Endonuclease III mutant Y82A, which is defective in carrying out DNA CT, shows only one regime for protein binding. Decreasing the temperature to 4 °C or including metallointercalators on the duplex, both of which should enhance base stacking and decrease DNA floppiness, leads to extending the effective length for DNA charge transport to ∼5300 bp or 1.8 μm. These results thus support DNA charge transport between repair proteins over kilobase distances. The results furthermore highlight the ability of DNA repair proteins to search the genome quickly and efficiently using DNA charge transport chemistry.

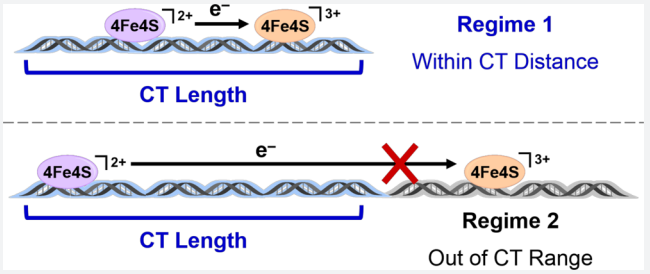

INTRODUCTION

Cellular oxidative stress, external UV irradiation, and environmental mutagens cause genomic lesions and base pair modifications in living organisms on the order of tens per cell per second.[1,2] Various repair mechanisms are present in biological systems to search and correct DNA lesions and mismatches, thereby upholding genomic integrity.[3,4] It is important that this repair be carried out quickly, before the damage can influence downstream processes or lead to mutations.[5,6] In humans, accumulation of mutations caused by defective DNA repair can lead to the proliferation of tumor cells and development of cancer.[7,8]

Recently, many DNA repair proteins have been found to possess redox-active [4Fe4S] clusters that may expedite their DNA damage search.[9−11] Experiments using DNA-modified electrodes show that these proteins all share a broad DNA-bound potential of ∼80 mV versus NHE, well below the potential at which DNA bases are oxidized.[12,13] Although these [4Fe4S] cluster repair proteins are typically present in cells in relatively low copy numbers,[14,15] they must find and repair thousands of mutagenic lesions within the 20 min doubling time of *Escherichia coli*.[16,17] Translocation is insufficient to explain the fast action of these proteins, especially when accounting for limitations of diffusion in the congested cellular environment.[16]

DNA-processing proteins containing [4Fe4S] clusters are found in archaea, bacteria, and eukaryotes.[18−23] Primases and polymerases containing [4Fe4S] clusters function as redox switches that control DNA replication processes.[24,25] Base excision repair proteins such as EndoIII, MutY, and uracil DNA glycosylase (UDG), as well as SF2 helicases XPD, and DinG contain redox-active [4Fe4S] clusters.[26−33] These [4Fe4S] clusters may play a vital functional role in the DNA damage search and repair scheme, though there is still much to be understood about how they function in biological systems.[34−37]

Recent experiments with DNA-modified Au electrodes and microscale thermophoresis (MST) suggest that the [4Fe4S] cluster acts as a redox-modulated affinity switch for DNA.[38] Using MST to quantify the binding affinity of DNA to EndoIII, EndoIII with an oxidized $[4Fe4S]^{3+}$ cluster was found to bind DNA 550-fold stronger than that with a reduced $[4Fe4S]^{2+}$ cluster.[38] Electrochemical experiments also demonstrated that binding to the anionic phosphate backbone of DNA shifts the

Received: August 14, 2018
Published: January 11, 2019

DOI: 10.1021/acscentsci.8b00566
ACS Cent. Sci. 2019, 5, 65−72

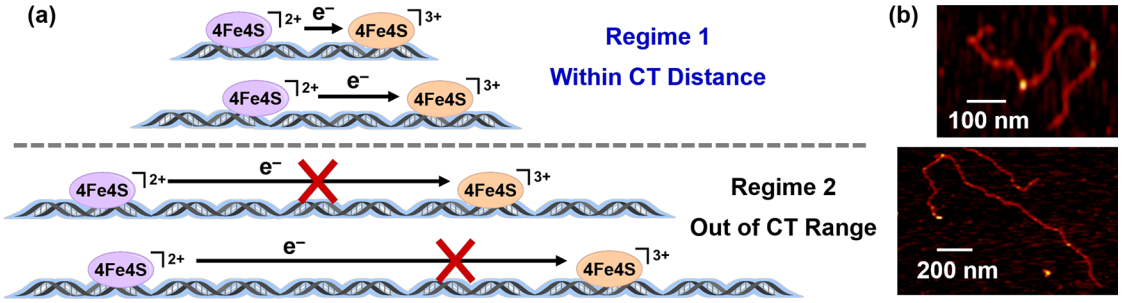

Figure 1. Quantifying the DNA charge transport length. (a) Model showing the implications of DNA CT length on the redox signaling capability between [4Fe4S] repair proteins and subsequently the lesion search process. (b) AFM images of two linear dsDNA. The one on the top is in the regime where the DNA length is shorter than the CT length, while the one on the bottom is in the regime where the DNA length is longer than the CT length.

redox potential of [4Fe4S] clusters in DNA repair proteins negative by about 200 mV.[39] This shift in redox potential corresponds to a change in the DNA-binding affinity that is similar to the values determined using MST.[40] The effect of binding to the polyanionic phosphate backbone of DNA contributes substantially to the shift in redox potential of the [4Fe4S] cluster in DNA repair proteins.[38,40] Previous experiments have demonstrated that changing buffer salts result in only small differences in redox potential.[41] Atomic force microscopy (AFM) experiments show that these proteins reduce and oxidize one another through a DNA-mediated redox signaling process, effectively allowing for [4Fe4S] cluster proteins to change one another's affinity to DNA.[11,38]

We have proposed that these proteins containing [4Fe4S] clusters utilize DNA charge transport (CT) as a means more rapidly and efficiently to search the genome for lesions. Using ultrafast spectroscopy and electrochemical experiments, DNA CT occurs rapidly through well stacked DNA in both the excited and ground states but is interrupted by lesions, mismatches, and other perturbations to the duplex base pair stacking.[42−44] Redox-active [4Fe4S] cluster repair proteins can utilize the disruption of DNA CT by lesions to screen the genome for DNA damage.[45,46] Inside cells, oxidative stress may oxidize the [4Fe4S] cluster of the proteins, or oxidize DNA bases that can then undergo CT with the protein.[47,48] When the proteins bind to the DNA polyanion, they are activated toward oxidation. Hence, they are more prone to bind to DNA and lose an electron in the process.[47] If there is no DNA damage, the electron can travel down the length of DNA and reduce the oxidized $[4Fe4S]^{3+}$ cluster of another repair protein, thereby decreasing its affinity and releasing it from DNA.[49] This released protein can then continue its search elsewhere.[48] This method, as a first step in the search process, allows for proteins to find DNA damage much faster than by translocation alone.[50] Incorporating DNA-mediated charge transport into the search, and assuming an effective DNA CT length of 200−500 bp between proteins, the time needed for [4Fe4S] cluster repair proteins to search for DNA damage sites shortens by at least an order of magnitude. By utilizing DNA CT in the DNA damage search process, the time needed for [4Fe4S] repair proteins to scan the entire genome is well within the time constraints of other biological processes.[16] One key advantage of a DNA CT supported search scheme is that electrons can travel through DNA across a heavily congested cellular environment in a relatively unhindered fashion on a nanosecond time scale,[50] as opposed to a search scheme utilizing only translocation by proteins that takes much longer to cover the same distance, and can be made even slower than 0.1−10 $\mu m^2/s$ in *E. coli* because the crowded cellular environment impedes movement.[16,51−53]

However, what is the distance over which DNA CT can proceed? Previously we have utilized a 100 bp dsDNA-modified electrode to demonstrate that DNA CT can occur over at least a distance of 34 nm.[54] Practical synthetic limitations have, however, precluded the examination of longer distances on electrodes, including those larger than the DNA duplex persistence length of 50 nm (150 bp).[55−58] In addition, extrapolation from experiments with shorter DNA on DNA-modified electrodes has been inadequate for predicting a maximum length because the rate of electron transfer is generally limited by the attachment to the electrode.[54] Moreover, photophysical experiments varying the length of DNA have shown an extremely shallow distance dependence for DNA CT, while the same synthetic limitations apply.[54,59]

AFM experiments allow for the interrogation under equilibrium conditions of DNA CT distance over 100 times longer than that used on DNA-modified electrodes, but cannot elucidate the kinetics of this process.[11,38] After proteins and DNA were allowed to interact, AFM is used to count the number of proteins bound on DNA.[60] The AFM experimental procedure does not change the population of proteins bound on DNA.[16] Previous AFM experiments demonstrate that DNA-mediated CT can occur between different proteins containing [4Fe4S] clusters.[16,47,48,50,60] Using our AFM assay to probe long-range signaling between proteins has, moreover, suggested that DNA CT might proceed over kilobase lengths.[11] Experimental data from these experiments suggest that DNA CT lowers the effective binding affinity of any pair of reduced and oxidized [4Fe4S] proteins relative to the affinity of a protein with oxidized $[4Fe4S]^{3+}$ that is not involved in DNA CT.[38] Thus, if new proteins bind to DNA with reduced $[4Fe4S]^{2+}$ clusters and are capable of DNA CT with a bound protein containing an oxidized $[4Fe4S]^{3+}$, the effective affinity of these proteins will be decreased relative to the oxidized $[4Fe4S]^{3+}$ protein alone.

If a maximum DNA CT length exists, we expect to detect two regimes in AFM experiments with different observable affinities for DNA−protein interactions: shorter DNA where all the proteins that bind are capable of DNA CT with another protein, and longer DNA where proteins can bind outside of maximum DNA CT distance of other proteins (Figure 1). In the shorter regime all of the proteins have decreased affinities relative to a lone oxidized $[4Fe4S]^{3+}$ protein, but in the longer regime many of the oxidized proteins will not have their affinity

DOI: 10.1021/acscentsci.8b00566
ACS Cent. Sci. 2019, 5, 65−72

decreased. As the DNA length increases beyond the maximum DNA CT length, the probability that two or more [4Fe4S] cluster proteins bind to DNA far enough away from one another to be outside of the range for DNA CT should increase, and the proportion of unperturbed $[4Fe4S]^{3+}$ binding should increase with it. With this in mind, we conducted experiments using DNA of different lengths and measured the binding of [4Fe4S] proteins to see if we could observe differences in the number of bound proteins per base pair and thereby determine the maximum effective length of DNA CT between two proteins. Within the context of our proposed model, the effective distance is defined as the length of DNA within which two proteins are able to influence their ensemble affinity to the DNA duplex via CT. Notably, the effective CT length is not determined by directly measuring the length of DNA in between the proteins given our inability to distinguish proteins in different redox states. We instead monitor the ensemble distribution of proteins on DNA after CT has occurred.

RESULTS

DNA CT Length of WT EndoIII at Room Temperature (RT). The number of proteins bound to DNA was counted using images collected using AFM techniques. The number of proteins bound to different lengths of DNA was used to determine the affinity of those proteins to DNA. AFM images were collected using double-stranded DNA of 1625, 1999, 2686, 3895, 5153, 5967, 7037, 7996, and 8922 bp in length prepared using PCR and plasmid excision methods (Scheme 1). The AFM results are summarized in Figure 2 and Figure S1. Two regimes are observed, designated by black and blue lines. The blue line, with a shallow slope, represents the regime where the DNA length is shorter than the CT length. Here the [4Fe4S] cluster proteins are within CT distance for all binding configurations. Increases in DNA length in this regime effectively add a lower affinity binding site, giving it a relatively shallow slope. The steeper black line represents the regime where DNA length is longer than the CT length. Here some [4Fe4S] cluster proteins are not within CT distance to communicate with each other. As the DNA CT length increases, the probability of [4Fe4S] cluster proteins not within the CT distance with each other increases, giving them a higher effective affinity and resulting in a steeper slope. Although the average number of bound proteins is less than one, the presence of DNA duplexes bound with 2 and 3 proteins shows that the binding of proteins to DNA of these lengths is influenced by DNA CT, and our data indicate that the prevalence of DNA with 2 and 3 proteins is suppressed by DNA CT. These data suggest that proteins in the 2+ and 3+ oxidation states within CT distance have a lower ensemble binding affinity than proteins that are isolated from each other. The point where the two regimes converge is the DNA length where it starts to become possible that proteins bind without experiencing DNA CT; we consider this the value for the maximum DNA CT length between proteins. At ambient temperatures, WT EndoIII exhibits a DNA CT length of 3509 ± 509 bp, or 1.192 ± 0.174 μm (Figure 2 and Figure S1), significantly longer than shown by previous measurements.

Scheme 1. Constructing Linear Double-Stranded DNA of Various Lengths by (a) Plasmid Excision Using SacI (Magenta) and (b) PCR Amplification Methods[a]

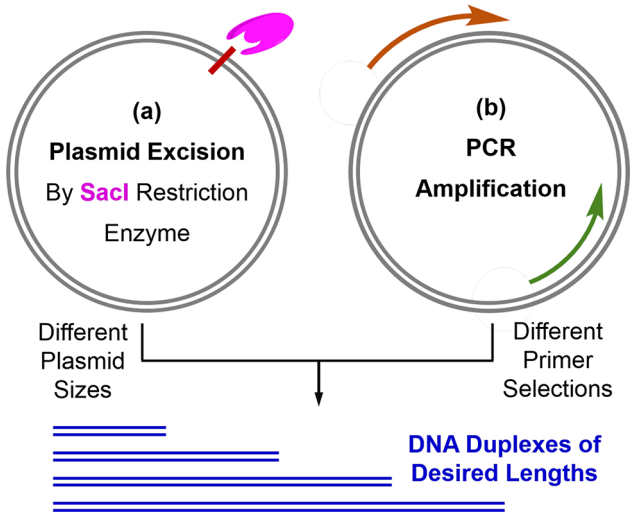

[a]The detailed protocols to prepare DNA duplexes of different lengths are presented in the SI, Methods section. See Table S1 for the primer sequences and plasmid templates used in the PCR amplification steps.

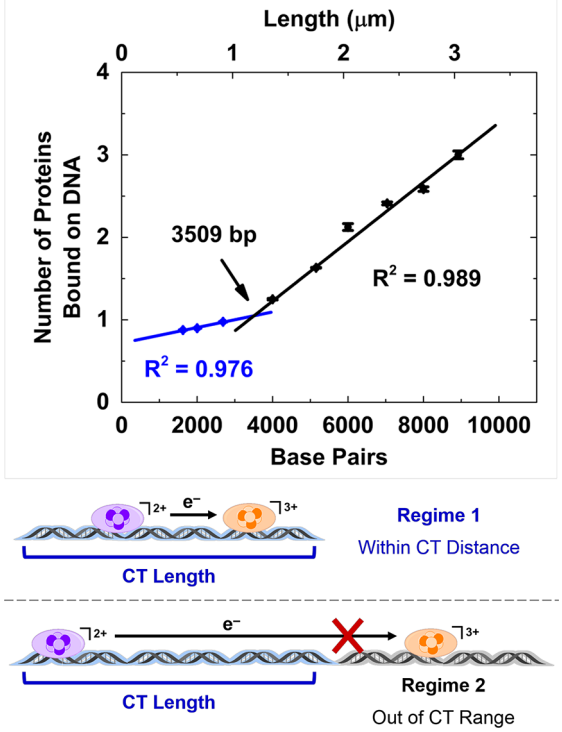

Figure 2. Measuring DNA-binding density of wild-type EndoIII at ambient temperature using atomic force microscopy. A sharp change in binding slope is observed at 3509 base pairs, or about 1.2 μm, that suggests the presence of two regimes for protein binding, one within the range for DNA CT (regime 1, blue), one outside of the range for CT (regime 2, black). 1310 DNA duplexes were analyzed from four independent preparations.

DNA CT Length of Y82A EndoIII Mutant at RT. To determine whether the observed slope change is in fact related to DNA CT, we performed control experiments with the Y82A EndoIII mutant that was previously characterized to be DNA CT-deficient with its enzymatic activity unperturbed.[16] The AFM results are summarized in Figure 3 with additional information in Figure S2. Only one regime is observed with no apparent change of slope as a function of DNA lengths. Since

DOI: 10.1021/acscentsci.8b00566
ACS Cent. Sci. 2019, 5, 65−72

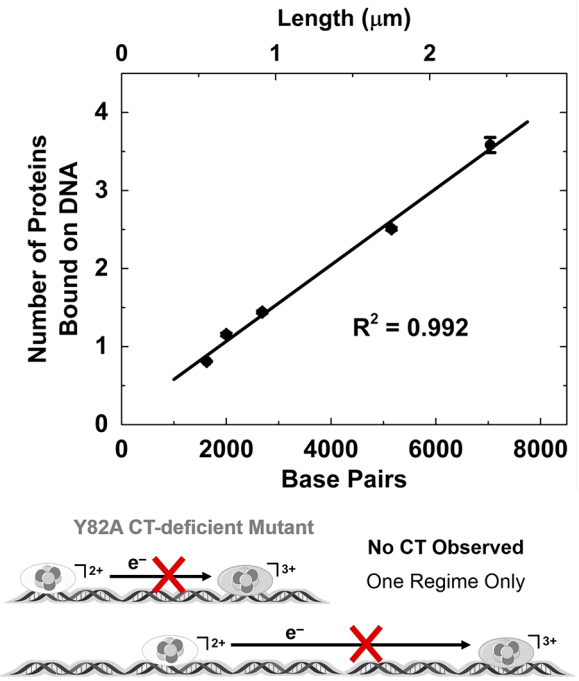

Figure 3. Measuring DNA-binding density of Y82A EndoIII mutant at ambient temperature using atomic force microscopy. No change in binding slope as a function of DNA lengths is observed, indicating the absence of DNA CT. As Y82A does not undergo redox signaling with each other via DNA CT, the DNA-binding affinity of Y82A is independent of each other. 272 DNA duplexes were analyzed from four independent preparations.

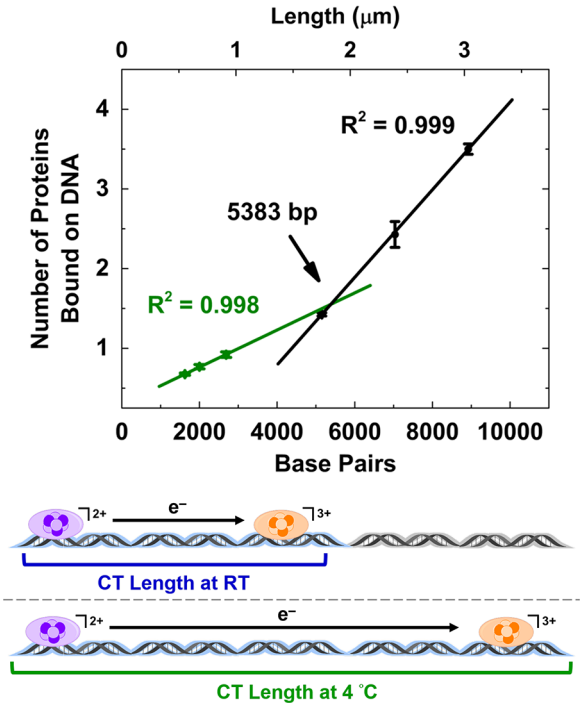

Figure 4. Measuring DNA-binding density of wild-type EndoIII at 4 °C using atomic force microscopy. A sharp change in binding slope occurs at 5383 base pairs, or about 1.8 μm, indicating that the DNA CT length observed at 4 °C is significantly longer than that at RT. 151 DNA duplexes were analyzed from four independent preparations.

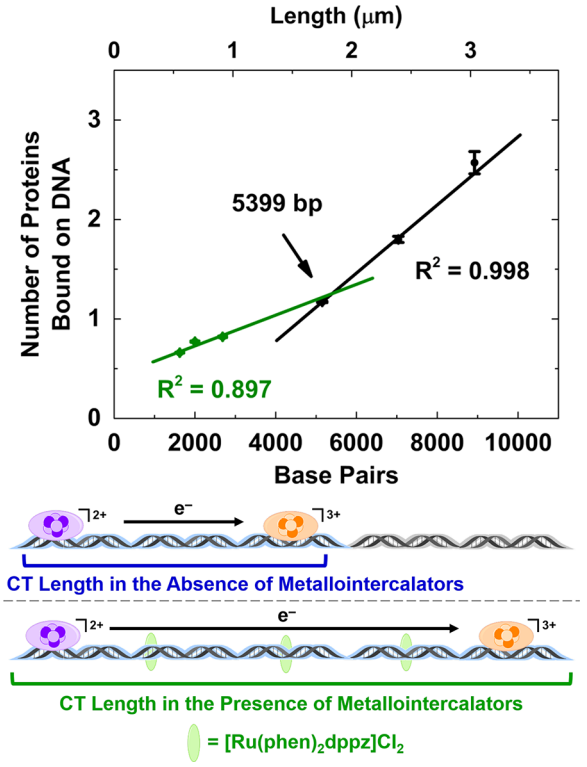

Figure 5. Measuring DNA-binding density of wild-type EndoIII in the presence of $[Ru(phen)_2dppz]Cl_2$ (50 μM) at ambient temperature using atomic force microscopy. A sharp change in binding slope occurs at 5399 base pairs, or about 1.8 μm, suggesting that metallointercalators lengthen the DNA CT length observed. 449 DNA duplexes were analyzed from four independent preparations.

Y82A does not exhibit DNA CT but remains otherwise the same as WT EndoIII,[61] the lack of the slope change in Figure 3 is consistent with the slope change observed for WT EndoIII in Figure 2 being a result of DNA CT. As Y82A does not undergo redox signaling with each other via DNA CT, the DNA-binding affinity of Y82A is independent of each other. Y82A does not exhibit DNA CT but remains otherwise the same as WT EndoIII.[12,61] Thus, these data in Figure 3 show that DNA CT deficiency is sufficient to eliminate the two-sloped feature observed in data collected with the wild-type protein in Figure 2, which suggests that the change in slope in the wild-type protein is a result of DNA CT.

DNA CT Length of WT EndoIII at 4 °C. To examine if the DNA CT length is temperature dependent, we conducted AFM experiments with samples prepared at colder temperatures. The AFM results are presented in Figure 4. At 4 °C, WT EndoIII exhibits a much longer DNA CT length (5383 ± 174 bp, or 1.830 ± 0.059 μm) than that measured at RT. This increase in DNA CT length is expected, as a decrease in temperature limits molecular motion; i.e., DNA will be less floppy.[62]

DNA CT Length of WT EndoIII at RT in the Presence of a Metallointercalator. To determine if the DNA CT length can be altered using molecular means, we conducted AFM experiments in the presence of $[Ru(phen)_2dppz]Cl_2$ (50 μM), which is a known metallointercalator.[63] The redox potential of the [4Fe4S] clusters in EndoIII is outside of the potential range at which the Ru intercalators are reduced or oxidized.[64] The AFM results are displayed in Figure 5 with additional information in Figure S3. The AFM experiments demonstrate that in the presence of 50 μM $[Ru(phen)_2dppz]Cl_2$ WT EndoIII exhibits a DNA CT length of 5399 ± 1732

DOI: 10.1021/acscentsci.8b00566
ACS Cent. Sci. 2019, 5, 65−72

bp, or 1.836 ± 0.589 μm (Figure 5 and Figure S3). This increase in DNA CT length is consistent with the increase in DNA stability upon intercalation of metal complexes.[63,65,66] Additionally, as one would expect, the results support the presence of π-stacked metallointercalators not impeding DNA CT.

DISCUSSION

Determining DNA CT Length Using AFM Experiments. This study aims to measure the effective maximum distance for DNA-mediated charge transport between proteins by monitoring changes in the affinity of [4Fe4S] proteins to DNA with increasing duplex length. An obvious change in slope occurs for EndoIII that is capable of DNA CT, but not for its CT-deficient mutant Y82A. Although the average number of proteins bound is less than one in some cases, these data show binding of the second and higher number of proteins is significantly decreased beyond what would be expected if the second (and higher) protein bound independently of the first, which shows that this aggregate value is taking into account the influence of DNA CT on binding affinity. We can therefore consider the change in slope a feature of proteins capable of DNA CT, which indicates that an increase in affinity with DNA length is shallow at shorter DNA distances and steep at longer DNA distances. Additionally, it is possible to modify the point at which this slope change occurs by changing the temperature and including DNA intercalators, both of which can change the stability of the duplex and the efficiency of DNA CT.

Understanding DNA CT Length Using an Equilibrium Binding Model. The data collected using AFM represent a snapshot of the proteins bound to DNA at equilibrium. Fitting a plot of the number of proteins per duplex from AFM data shows an intersection of two different regimes, whereby increasing the length of DNA differently affects the increase in affinity of proteins for the additional binding sites. We interpret this change in slope as indicative of a maximum CT length at ambient temperature of 3509 ± 509 bp, or 1.192 ± 0.174 μm, which is not observed in CT-deficient proteins.

To further understand these data, an equilibrium model was developed to help describe the DNA-binding behavior of proteins that are capable of DNA CT (see the SI, Methods). The first protein that binds to DNA is insensitive to DNA CT, and the affinity we observe is dependent on the oxidation state of the protein [4Fe4S] cluster.[38] The dissociation constant for EndoIII with a reduced $[4Fe4S]^{2+}$ cluster was previously determined by MST to be 1.3×10^{-4} per bp, and EndoIII with an oxidized $[4Fe4S]^{3+}$ cluster has an affinity of 2.3×10^{-7} per bp.[38] These values were used as inputs of our model to estimate the percent of oxidized $[4Fe4S]^{3+}$ clusters in our sample, 5.6 ± 1.7% (see the SI, Methods). Modeling the binding of additional proteins to incorporate contributions of DNA CT allows us then to determine the effective dissociation constant for proteins undergoing CT, which is $4.3 \times 10^{-5} \pm 1 \times 10^{-5}$ per bp, a decrease in affinity of over 2 orders of magnitude compared to the oxidized protein that results from electron transfer with a nearby reduced protein.

Importantly, using these values for the percent of oxidized [4Fe4S] clusters and the effective affinity of proteins undergoing CT, we may simulate the data collected by AFM (Figure S4). Results from our theoretical calculations show the same trends as the collected data, including the two regimes above and below the effective CT distance with different slopes. The intersection of these two regimes in the simulated data provides a maximum CT length of 2990 bp, which agrees well with the experimental data and further strengthens the claim that the presence of two regimes in our experimental data is due to the effect of DNA CT on the DNA-binding affinity of redox-active proteins.

Other experimental conditions yield similar values for the percent of oxidized protein and decrease in affinity due to charge transport but show dramatic differences in the length of CT (Table S3). Fitting similar data collected from a CT-deficient Y82A EndoIII mutant does not show any measurable CT distance, which is also supported by simulated data using the same model (Figure S4). Decreasing the temperature at which proteins are incubated with DNA to 4 °C increases the measured CT length to 5383 ± 174 bp. As temperature decreases, the persistence length of the DNA backbone increases.[62] The incorporation of the metallointercalator $[Ru(phen)_2dppz]Cl_2$, which is known to stabilize DNA duplexes,[63,65,66] increases the CT length to 5399 ± 1732 bp. These results suggest that as the rigidity of DNA increases, the CT length also increases, likely due to stabilizing the DNA duplex in a more CT-favorable state.

Biological Implications of DNA CT Length. Knowing the length that DNA CT can occur between proteins allows for predictions to be made about the effectiveness of DNA CT in increasing the efficiency of DNA damage repair. In our initial prediction, by assuming a DNA CT length of 200−500 bp, the time needed to search the *E. coli* genome decreases by an order of magnitude over calculations excluding DNA CT.[16] The current AFM study indicates a DNA CT length of 3500 bp, so that the efficiency of the genome lesion search can significantly increase further or require fewer involved proteins. Incorporating the data from this AFM study will be useful for better modeling of the DNA damage search and repair process and the role that such long-distance CT may play.

Now we consider how DNA CT plays a role in biological systems using *E. coli* strain as an example. *E. coli* K-12 strain has a genome size of 4 639 221 bp.[67] Dividing the number of total bp by the measured DNA CT length of 3509 bp per protein gives a rough calculation that 1322 [4Fe4S] repair proteins are needed to place the whole *E. coli* genome within DNA CT range of these [4Fe4S] repair proteins. Although individually these [4Fe4S] repair proteins may be present in cells in low copy numbers, previous studies have demonstrated that [4Fe4S] cluster proteins from different repair pathways can signal with each other *in vivo*.[11] Summing up the copy numbers of EndoIII, MutY, and DinG gives an estimate of the total number of known [4Fe4S]-containing DNA repair proteins in *E. coli* of at least about 1100.[15] We have measured the redox potential of multiple proteins, and find that they are all close to one another, which suggests that they can all influence one another's binding affinity through DNA CT. However, it is not clear how other differences within the cell may affect the search and repair process. With more [4Fe4S] proteins yet to be described, together these relevant [4Fe4S] repair proteins may participate in and enable a genome-wide search for DNA lesions via DNA CT.

CONCLUSIONS

In this report, we utilized atomic force microscopy and an equilibrium binding model to study the effective DNA charge transport length between oxidized and reduced Endonuclease III, a DNA repair protein carrying a redox-active [4Fe4S]

DOI: 10.1021/acscentsci.8b00566
ACS Cent. Sci. 2019, 5, 65−72

cluster. AFM data reveal two regimes of DNA-binding behavior. In one regime, where the DNA length is shorter than the CT length, a copy of EndoIII in the reduced $[4Fe4S]^{2+}$ state bound on DNA modulates the DNA-binding affinity of a second copy of EndoIII with an oxidized $[4Fe4S]^{3+}$ cluster, no matter where the second copy is bound on DNA. Because the two EndoIII proteins are always within CT distance, their effective affinity for DNA is averaged. In another regime where the DNA length is longer than the CT length, there now exist binding sites where proteins with oxidized $[4Fe4S]^{3+}$ clusters can bind outside of CT range with a higher effective affinity. As the DNA length increases, the probability of additional EndoIII binding outside of CT distance with higher effective affinity increases. Modeling allowed us to extract the maximum effective DNA CT length between proteins, which we found to be 3509 base pairs, or about 1.2 μm at ambient temperature. A mechanistic understanding of this long-range DNA CT now requires exploration by theorists.[68] The DNA CT length can be changed with temperature and by stabilizing DNA with metallointercalators. These data suggest that the effective DNA CT length can be controlled by its environment, which has interesting implications for both biological systems and technology that use DNA CT. An effective DNA CT length this long enables a fast genome lesion search scheme via long-range redox signaling.

EXPERIMENTAL SECTION

General Procedures. Chemicals were obtained from commercial sources (Sigma-Aldrich, Fisher Scientific, VWR, and New England Biolabs) and used without further purification unless otherwise specified. DNA primer sequences were purchased from Integrated DNA Technologies, purified by high performance liquid chromatography (HPLC, HP 1100, Agilent), characterized using matrix-assisted laser desorption ionization (MALDI) mass spectrometry using an Autoflex MALDI TOF/TOF instrument (Bruker), and quantified using a 100 Bio UV−vis spectrophotometer (Cary, Agilent) as described previously.[69−73] Phosphate buffer (pH 7.0, 5 mM NaH_2PO_4, 50 mM NaCl) was prepared using Milli-Q water (>18 MΩ cm). Experiments performed were replicated at least three times using different samples, and data presented are from representative trials. The SI, Methods section, contains protocols for overexpression and purification of wild-type EndoIII and Y82A mutant and synthesis of DNA duplexes of various lengths (Table S1).

AFM Experiments. AFM was conducted following protocols reported previously.[11,38,60,61] Briefly, mica surfaces were freshly cleaved with tape. Protein stock solution (100 nM) contained either WT EndoIII or Y82A mutant in phosphate buffer (pH 7.0, 5 mM NaH_2PO_4, 50 mM NaCl). Stock DNA solution (9 μM bp) contained the mixture of DNA duplexes of various lengths in Tris elution buffer (EB, 10 mM Tris-HCl, pH 8.5, Qiagen). A solution (23.5 μL) with a final protein concentration (12 nM) and a final total DNA concentration (5 μM bp) was prepared and incubated at ambient temperature for 1 h or 4 °C for 2 h to allow for the loading of protein onto DNA to reach equilibrium while minimizing cluster degradation. For experiments with metallointercalators, a final concentration of 50 μM $[Ru(phen)_2dppz]Cl_2$ was added. $MgCl_2$ (200 mM, 1.5 μL per 25 μL total volume) was added to promote DNA adsorption on mica for AFM experiments. After pipetting 12.5 μL of DNA/protein/$MgCl_2$ solution onto a freshly cleaved mica surface and incubating for 2 min, a continuous stream of Milli-Q water (2 mL) was slowly poured over the top portion of the modified mica surface while holding the piece of mica in a vertical position to linearize the DNA. A piece of lint-free wipe was used to dab dry the bottom edge of the mica surface. The surface was dried using a stream of N_2 flowing in the same direction as the water rinse for 2 min. No significant safety hazards were encountered.

AFM Instrumentation. FESPA-V2 AFM tapping mode probes (Bruker Nano, Inc.) with a mean force constant of 2.8 N/m and a mean resonance frequency of 75 kHz were used in a MFP-3D AFM instrument (Asylum Research). Images were captured in air with scan areas of 5 × 5 μm^2 in tapping mode at a scan rate of 1 Hz to obtain images of quality high enough for AFM assay analysis (512 pixels/line, 512 lines/image). Over 1000 AFM images were collected, and over 2000 DNA strands were analyzed blind as described previously.[38]

AFM Image Analysis. WSxM software (Igor Pro) was used to analyze DNA contour lengths and height profiles of the proteins as described previously.[38] DNA and proteins were identified using the relative differential height profiles between protein and DNA. For each data set, images from at least three independent samples were analyzed. Distinguishable DNA and proteins were counted by hand. Duplexes that were overlapped, indistinguishable, or cut off by the edge of the image were excluded from the counting procedure. Binding density is defined as the number of the proteins bound on a DNA duplex. Data presented are from representative trials, and error bars represent standard error of all trials based on the total number of proteins observed (Table S2, n > 200 for all experiments).

ASSOCIATED CONTENT

Supporting Information

The Supporting Information is available free of charge on the ACS Publications website at DOI: 10.1021/acscentsci.8b00566.

Supplemental methods, data, and figures including schematics, protein counts, box plots, UV−vis spectra, and AFM image (PDF)

AUTHOR INFORMATION

Corresponding Author

*E-mail: jkbarton@caltech.edu.

ORCID

Edmund C. M. Tse: 0000-0002-9313-1290

Jacqueline K. Barton: 0000-0001-9883-1600

Present Addresses

†E.C.M.T.: Department of Chemistry, The University of Hong Kong, Pokfulam Road, Hong Kong SAR.

‡T.J.Z.: Department of Chemistry and Chemical Biology, Harvard University, Cambridge, MA 02138, USA.

Notes

The authors declare no competing financial interest.

ACKNOWLEDGMENTS

We gratefully recognize the NIH (GM126904) for financial support. E.C.M.T. appreciates the Croucher Foundation for a postdoctoral fellowship. T.J.Z. is an NSF fellow (DGE-1144469). S.B. acknowledges Joseph L. Koo and Helen C.

DOI: 10.1021/acscentsci.8b00566
ACS Cent. Sci. 2019, 5, 65−72

Koo for a student undergraduate research fellowship. We thank Dr. Adam N. Boynton and Kelsey M. Boyle for providing metallointercalators for this study. We are also grateful to the Caltech Center for the Chemistry of Cellular Signaling for instrumentation. This research was enabled from the use of the Autoflex MALDI TOF in the Caltech CCE Multiuser Mass Spectrometry Laboratory, acquired with funds from the DOW corporation (CCEC.DOWINSTR). AFM experiments were carried out at the Molecular Materials Research Center of the Beckman Institute of the California Institute of Technology.

REFERENCES

(1) Jackson, S. P.; Bartek, J. The DNA-damage Response in Human Biology and Disease. *Nature* **2009**, *461* (7267), 1071−1078.
(2) Lindahl, T.; Barnes, D. E. Repair of Endogenous DNA Damage. *Cold Spring Harbor Symp. Quant. Biol.* **2000**, *65*, 127−134.
(3) Hoeijmakers, J. H. J. Genome Maintenance Mechanisms for Preventing Cancer. *Nature* **2001**, *411* (6835), 366−374.
(4) Sancar, A.; Lindsey-Boltz, L. A.; Unsal-Kacmaz, K.; Linn, S. Molecular Mechanisms of Mammalian DNA Repair and the DNA Damage Checkpoints. *Annu. Rev. Biochem.* **2004**, *73*, 39−85.
(5) David, S. S.; O'Shea, V. L.; Kundu, S. Base-excision Repair of Oxidative DNA Damage. *Nature* **2007**, *447* (7147), 941−950.
(6) Marteijn, J. A.; Lans, H.; Vermeulen, W.; Hoeijmakers, J. H. J. Understanding Nucleotide Excision Repair and its Roles in Cancer and Ageing. *Nat. Rev. Mol. Cell Biol.* **2014**, *15* (7), 465−481.
(7) Tubbs, A.; Nussenzweig, A. Endogenous DNA Damage as a Source of Genomic Instability in Cancer. *Cell* **2017**, *168* (4), 644.
(8) Knijnenburg, T. A.; Wang, L.; Zimmermann, M. T.; Chambwe, N.; Gao, G. F.; Cherniack, A. D.; Fan, H.; Shen, H.; Way, G. P.; Greene, C. S.; et al. Genomic and Molecular Landscape of DNA Damage Repair Deficiency across The Cancer Genome Atlas. *Cell Rep.* **2018**, *23* (1), 239−254.
(9) Fuss, J. O.; Tsai, C.-L.; Ishida, J. P.; Tainer, J. A. Emerging critical roles of Fe−S clusters in DNA replication and repair. *Biochim. Biophys. Acta, Mol. Cell Res.* **2015**, *1853* (6), 1253.
(10) Rouault, T. A. Iron-sulfur Proteins Hiding in Plain Sight. *Nat. Chem. Biol.* **2015**, *11* (7), 442−445.
(11) Grodick, M. A.; Segal, H. M.; Zwang, T. J.; Barton, J. K. DNA-Mediated Signaling by Proteins with 4Fe-4S Clusters is Necessary for Genomic Integrity. *J. Am. Chem. Soc.* **2014**, *136* (17), 6470−6478.
(12) Boal, A. K.; Yavin, E.; Lukianova, O. A.; O'Shea, V. L.; David, S. S.; Barton, J. K. DNA-Bound Redox Activity of DNA Repair Glycosylases Containing [4Fe-4S] Clusters. *Biochemistry* **2005**, *44* (23), 8397−8407.
(13) Kelley, S. O.; Barton, J. K. Electron Transfer Between Bases in Double Helical DNA. *Science* **1999**, *283* (5400), 375.
(14) Demple, B.; Harrison, L. Repair of Oxidative Damage to DNA: Enzymology and Biology. *Annu. Rev. Biochem.* **1994**, *63*, 915−948.
(15) Li, G.-W.; Burkhardt, D.; Gross, C.; Weissman, J. S. Quantifying Absolute Protein Synthesis Rates Reveals Principles Underlying Allocation of Cellular Resources. *Cell* **2014**, *157* (3), 624−635.
(16) Boal, A. K.; Genereux, J. C.; Sontz, P. A.; Gralnick, J. A.; Newman, D. K.; Barton, J. K. Redox Signaling between DNA Repair Proteins for Efficient Lesion Detection. *Proc. Natl. Acad. Sci. U. S. A.* **2009**, *106* (36), 15237−15242.
(17) Lee, H.; Popodi, E.; Tang, H.; Foster, P. L. Rate and molecular spectrum of spontaneous mutations in the bacterium Escherichia coli as determined by whole-genome sequencing. *Proc. Natl. Acad. Sci. U. S. A.* **2012**, *109* (41), E2774−E2783.
(18) Agarwalla, S.; Stroud, R. M.; Gaffney, B. J. Redox Reactions of the Iron-Sulfur Cluster in a Ribosomal RNA Methyltransferase, RumA: OPTICAL AND EPR STUDIES. *J. Biol. Chem.* **2004**, *279* (33), 34123−34129.
(19) Netz, D. J. A.; Stith, C. M.; Stümpfig, M.; Köpf, G.; Vogel, D.; Genau, H. M.; Stodola, J. L.; Lill, R.; Burgers, P. M. J.; Pierik, A. J. Eukaryotic DNA polymerases require an iron-sulfur cluster for the formation of active complexes. *Nat. Chem. Biol.* **2012**, *8* (1), 125.
(20) Cunningham, R. P.; Asahara, H.; Bank, J. F.; Scholes, C. P.; Salerno, J. C.; Surerus, K.; Munck, E.; McCracken, J.; Peisach, J.; Emptage, M. H. Endonuclease III is an Iron-sulfur Protein. *Biochemistry* **1989**, *28* (10), 4450−4455.
(21) Thayer, M. M.; Ahern, H.; Xing, D.; Cunningham, R. P.; Tainer, J. A. Novel DNA Binding Motifs in the DNA Repair Enzyme Endonuclease III Crystal Structure. *EMBO J.* **1995**, *14* (16), 4108−4120.
(22) Chepanoske, C. L.; Golinelli, M.-P.; Williams, S. D.; David, S. S. Positively Charged Residues within the Iron−Sulfur Cluster Loop of E. coli MutY Participate in Damage Recognition and Removal. *Arch. Biochem. Biophys.* **2000**, *380* (1), 11−19.
(23) Brinkmeyer, M. K.; David, S. S. Distinct Functional Consequences of MUTYH Variants Associated with Colorectal Cancer: Damaged DNA Affinity, Glycosylase Activity and Interaction with PCNA and Hus1. *DNA Repair* **2015**, *34*, 39−51.
(24) O'Brien, E.; Holt, M. E.; Thompson, M. K.; Salay, L. E.; Ehlinger, A. C.; Chazin, W. J.; Barton, J. K. The [4Fe4S] Cluster of Human DNA Primase Functions as a Redox Switch using DNA Charge Transport. *Science* **2017**, *355* (6327), 813−822.
(25) Bartels, P. L.; Stodola, J. L.; Burgers, P. M. J.; Barton, J. K. A Redox Role for the [4Fe4S] Cluster of Yeast DNA Polymerase *δ*. *J. Am. Chem. Soc.* **2017**, *139* (50), 18339−18348.
(26) Engstrom, L. M.; Brinkmeyer, M. K.; Ha, Y.; Raetz, A. G.; Hedman, B.; Hodgson, K. O.; Solomon, E. I.; David, S. S. A Zinc Linchpin Motif in the MUTYH Glycosylase Interdomain Connector is Required for Efficient Repair of DNA Damage. *J. Am. Chem. Soc.* **2014**, *136* (22), 7829−7832.
(27) Porello, S. L.; Cannon, M. J.; David, S. S. A Substrate Recognition Role for the [4Fe-4S]2+ Cluster of the DNA Repair Glycosylase MutY. *Biochemistry* **1998**, *37* (18), 6465−6475.
(28) Pope, M. A.; David, S. S. DNA Damage Recognition and Repair by the Murine MutY Homologue. *DNA Repair* **2005**, *4* (1), 91−102.
(29) Fromme, J. C.; Verdine, G. L. Structure of a Trapped Endonuclease III−DNA Covalent Intermediate. *EMBO J.* **2003**, *22* (13), 3461−3471.
(30) O'Handley, S.; Scholes, C. P.; Cunningham, R. P. Endonuclease III Interactions with DNA Substrates. 1. Binding and Footprinting Studies with Oligonucleotides Containing a Reduced Apyrimidinic Site. *Biochemistry* **1995**, *34* (8), 2528−2536.
(31) Kuo, C.; McRee, D.; Fisher, C.; O'Handley, S.; Cunningham, R.; Tainer, J. Atomic Structure of the DNA Repair [4Fe-4S] Enzyme Endonuclease III. *Science* **1992**, *258* (5081), 434−440.
(32) Boal, A. K.; Yavin, E.; Barton, J. K. DNA Repair Glycosylases with a [4Fe-4S] Cluster: A Redox Cofactor for DNA-mediated Charge Transport? *J. Inorg. Biochem.* **2007**, *101* (11−12), 1913−1921.
(33) Fan, L.; Fuss, J. O.; Cheng, Q. J.; Arvai, A. S.; Hammel, M.; Roberts, V. A.; Cooper, P. K.; Tainer, J. A. XPD Helicase Structures and Activities: Insights into the Cancer and Aging Phenotypes from XPD Mutations. *Cell* **2008**, *133* (5), 789−800.
(34) Lukianova, O. A.; David, S. S. A Role for Iron−sulfur Clusters in DNA Repair. *Curr. Opin. Chem. Biol.* **2005**, *9* (2), 145−151.
(35) Rouault, T. A.; Tong, W.-H. Iron-sulphur Cluster Biogenesis and Mitochondrial Iron Homeostasis. *Nat. Rev. Mol. Cell Biol.* **2005**, *6* (4), 345−351.
(36) Rouault, T. A. Mammalian Iron-sulphur Proteins: Novel Insights into Biogenesis and Function. *Nat. Rev. Mol. Cell Biol.* **2015**, *16* (1), 45−55.
(37) Veatch, J. R.; McMurray, M. A.; Nelson, Z. W.; Gottschling, D. E. Mitochondrial Dysfunction Leads to Nuclear Genome Instability via an Iron-Sulfur Cluster Defect. *Cell* **2009**, *137* (7), 1247−1258.
(38) Tse, E. C. M.; Zwang, T. J.; Barton, J. K. The Oxidation State of [4Fe4S] Clusters Modulates the DNA-Binding Affinity of DNA Repair Proteins. *J. Am. Chem. Soc.* **2017**, *139* (36), 12784−12792.
(39) Gorodetsky, A. A.; Boal, A. K.; Barton, J. K. Direct Electrochemistry of Endonuclease III in the Presence and Absence of DNA. *J. Am. Chem. Soc.* **2006**, *128* (37), 12082−12083.

DOI: 10.1021/acscentsci.8b00566
ACS Cent. Sci. 2019, 5, 65−72

(40) Bartels, P. L.; Zhou, A.; Arnold, A. R.; Nuñez, N. N.; Crespilho, F. N.; David, S. S.; Barton, J. K. Electrochemistry of the [4Fe4S] Cluster in Base Excision Repair Proteins: Tuning the Redox Potential with DNA. *Langmuir* **2017**, *33* (10), 2523−2530.
(41) McDonnell, K. J.; Chemler, J. A.; Bartels, P. L.; O'Brien, E.; Marvin, M. L.; Ortega, J.; Stern, R. H.; Raskin, L.; Li, G.-M.; Sherman, D. H.; et al. A human MUTYH variant linking colonic polyposis to redox degradation of the [4Fe4S]2+ cluster. *Nat. Chem.* **2018**, *10* (8), 873.
(42) Murphy, C.; Arkin, M.; Jenkins, Y.; Ghatlia, N.; Bossmann, S.; Turro, N.; Barton, J. Long-range photoinduced electron transfer through a DNA helix. *Science* **1993**, *262* (5136), 1025−1029.
(43) Wan, C.; Fiebig, T.; Kelley, S. O.; Treadway, C. R.; Barton, J. K.; Zewail, A. H. Femtosecond dynamics of DNA-mediated electron transfer. *Proc. Natl. Acad. Sci. U. S. A.* **1999**, *96* (11), 6014−6019.
(44) Arkin, M. R.; Stemp, E. D. A.; Holmlin, R. E.; Barton, J. K.; Hörmann, A.; Olson, E. J. C.; Barbara, P. F. Rates of DNA-Mediated Electron Transfer Between Metallointercalators. *Science* **1996**, *273* (5274), 475.
(45) Sontz, P. A.; Muren, N. B.; Barton, J. K. DNA Charge Transport for Sensing and Signaling. *Acc. Chem. Res.* **2012**, *45* (10), 1792−1800.
(46) Merino, E. J.; Boal, A. K.; Barton, J. K. Biological Contexts for DNA Charge Transport Chemistry. *Curr. Opin. Chem. Biol.* **2008**, *12* (2), 229−237.
(47) Grodick, M. A.; Muren, N. B.; Barton, J. K. DNA Charge Transport within the Cell. *Biochemistry* **2015**, *54* (4), 962−973.
(48) Arnold, A. R.; Grodick, M. A.; Barton, J. K. DNA Charge Transport: from Chemical Principles to the Cell. *Cell Chem. Biol.* **2016**, *23* (1), 183−197.
(49) Núñez, M. E.; Holmquist, G. P.; Barton, J. K. Evidence for DNA Charge Transport in the Nucleus. *Biochemistry* **2001**, *40* (42), 12465.
(50) Genereux, J. C.; Boal, A. K.; Barton, J. K. DNA-Mediated Charge Transport in Redox Sensing and Signaling. *J. Am. Chem. Soc.* **2010**, *132* (3), 891.
(51) Phillips, R.; Kondev, J.; Theriot, J.; Orme, N. *Physical Biology of the Cell*; Garland Science: New York, 2013.
(52) Nenninger, A.; Mastroianni, G.; Mullineaux, C. W. Size Dependence of Protein Diffusion in the Cytoplasm of Escherichia coli. *J. Bacteriol.* **2010**, *192* (18), 4535−4540.
(53) Kumar, M.; Mommer, M. S.; Sourjik, V. Mobility of Cytoplasmic, Membrane, and DNA-Binding Proteins in Escherichia coli. *Biophys. J.* **2010**, *98* (4), 552−559.
(54) Slinker, J. D.; Muren, N. B.; renfrew, S. E.; Barton, J. K. DNA Charge Transport over 34 nm. *Nat. Chem.* **2011**, *3*, 228−233.
(55) Taylor, W. H.; Hagerman, P. J. Application of the method of phage T4 DNA ligase-catalyzed ring-closure to the study of DNA structure: II. NaCl-dependence of DNA flexibility and helical repeat. *J. Mol. Biol.* **1990**, *212* (2), 363−376.
(56) Bustamante, C.; Marko, J.; Siggia, E.; Smith, S. Entropic elasticity of lambda-phage DNA. *Science* **1994**, *265* (5178), 1599−1600.
(57) Hagerman, P. J. Flexibility of DNA. *Annu. Rev. Biophys. Biophys. Chem.* **1988**, *17* (1), 265−286.
(58) Smith, S.; Finzi, L.; Bustamante, C. Direct mechanical measurements of the elasticity of single DNA molecules by using magnetic beads. *Science* **1992**, *258* (5085), 1122−1126.
(59) Zwang, T. J.; Tse, E. C. M.; Barton, J. K. Sensing DNA through DNA Charge Transport. *ACS Chem. Biol.* **2018**, *13* (7), 1799−1809.
(60) Sontz, P. A.; Mui, T. P.; Fuss, J. O.; Tainer, J. A.; Barton, J. K. DNA Charge Transport as a First Step in Coordinating the Detection of Lesions by Repair Proteins. *Proc. Natl. Acad. Sci. U. S. A.* **2012**, *109* (6), 1856−1861.
(61) Romano, C. A.; Sontz, P. A.; Barton, J. K. Mutants of the Base Excision Repair Glycosylase, Endonuclease III: DNA Charge Transport as a First Step in Lesion Detection. *Biochemistry* **2011**, *50* (27), 6133−6145.
(62) Geggier, S.; Kotlyar, A.; Vologodskii, A. Temperature dependence of DNA persistence length. *Nucleic Acids Res.* **2011**, *39* (4), 1419−1426.
(63) Song, H.; Kaiser, J. T.; Barton, J. K. Crystal structure of Δ-[Ru(bpy)2dppz]2+ bound to mismatched DNA reveals side-by-side metalloinsertion and intercalation. *Nat. Chem.* **2012**, *4* (8), 615−620.
(64) Gorodetsky, A. A.; Barton, J. K. Electrochemistry using self-assembled DNA monolayers on highly oriented pyrolytic graphite. *Langmuir* **2006**, *22*, 7917−7922.
(65) Jennette, K. W.; Lippard, S. J.; Vassiliades, G. A.; Bauer, W. R. Metallointercalation Reagents. 2-Hydroxyethanethiolato(2,2′,2″-terpyridine)-platinum(II) Monocation Binds Strongly to DNA By Intercalation. *Proc. Natl. Acad. Sci. U. S. A.* **1974**, *71* (10), 3839−3843.
(66) Kielkopf, C. L.; Erkkila, K. E.; Hudson, B. P.; Barton, J. K.; Rees, D. C. Structure of a photoactive rhodium complex intercalated into DNA. *Nat. Struct. Biol.* **2000**, *7*, 117−121.
(67) Blattner, F. R.; Plunkett, G.; Bloch, C. A.; Perna, N. T.; Burland, V.; Riley, M.; Collado-Vides, J.; Glasner, J. D.; Rode, C. K.; Mayhew, G. F.; et al. The Complete Genome Sequence of Escherichia coli K-12. *Science* **1997**, *277* (5331), 1453−1462.
(68) Beratan, D. N.; Naaman, R.; Waldeck, D. H. Charge and spin transport through nucleic acids. *Curr. Opin. Electrochem.* **2017**, *4* (1), 175.
(69) Kelley, S. O.; Barton, J. K.; Jackson, N. M.; Hill, M. G. Electrochemistry of Methylene Blue Bound to a DNA-Modified Electrode. *Bioconjugate Chem.* **1997**, *8* (1), 31−37.
(70) Kelley, S. O.; Jackson, N. M.; Hill, M. G.; Barton, J. K. Long-Range Electron Transfer through DNA Films. *Angew. Chem., Int. Ed.* **1999**, *38* (7), 941−945.
(71) Slinker, J. D.; Muren, N. B.; Gorodetsky, A. A.; Barton, J. K. Multiplexed DNA-Modified Electrodes. *J. Am. Chem. Soc.* **2010**, *132* (8), 2769−2774.
(72) Boon, E. M.; Barton, J. K. DNA Electrochemistry as a Probe of Base Pair Stacking in A-, B-, and Z-Form DNA. *Bioconjugate Chem.* **2003**, *14* (6), 1140−1147.
(73) Zwang, T. J.; Tse, E. C. M.; Zhong, D.; Barton, J. K. A Compass at Weak Magnetic Fields Using Thymine Dimer Repair. *ACS Cent. Sci.* **2018**, *4* (3), 405−412.

DOI: 10.1021/acscentsci.8b00566
ACS Cent. Sci. 2019, 5, 65−72